ANNUAL REVIEWS

Annual Review of Biomedical Engineering

Bioelectronic Sensor Nodes for the Internet of Bodies

Baibhab Chatterjee,[1,2] Pedram Mohseni,[3] and Shreyas Sen[1]

[1] Elmore Family School of Electrical and Computer Engineering and Center for Internet of Bodies (C-IoB), Purdue University, West Lafayette, Indiana, USA; email: shreyas@purdue.edu

[2] Department of Electrical and Computer Engineering, University of Florida, Gainesville, Florida, USA

[3] Department of Electrical, Computer and Systems Engineering and Institute for Smart, Secure, and Connected Systems (ISSACS), Case Western Reserve University, Cleveland, Ohio, USA

Annu. Rev. Biomed. Eng. 2023. 25:101–29

First published as a Review in Advance on March 13, 2023

The *Annual Review of Biomedical Engineering* is online at bioeng.annualreviews.org

https://doi.org/10.1146/annurev-bioeng-110220-112448

Keywords

biosensors, Internet of Bodies, IoB, Internet of Things, IoT, sensing, in-sensor analytics, computation, communication, security, powering

Abstract

Energy-efficient sensing with physically secure communication for biosensors on, around, and within the human body is a major area of research for the development of low-cost health care devices, enabling continuous monitoring and/or secure perpetual operation. When used as a network of nodes, these devices form the Internet of Bodies, which poses challenges including stringent resource constraints, simultaneous sensing and communication, and security vulnerabilities. Another major challenge is to find an efficient on-body energy-harvesting method to support the sensing, communication, and security submodules. Due to limitations in the amount of energy harvested, we require a reduction in energy consumed per unit information, making the use of in-sensor analytics and processing imperative. In this article, we review the challenges and opportunities of low-power sensing, processing, and communication with possible powering modalities for future biosensor nodes. Specifically, we analyze, compare, and contrast (*a*) different sensing mechanisms such as voltage/current domain versus time domain, (*b*) low-power, secure communication modalities including wireless techniques and human body communication, and (*c*) different powering techniques for wearable devices and implants.

Contents

1. INTRODUCTION

In today's data-driven world, modern medical devices and biosensor nodes benefit from seamless connectivity, capturing valuable patient-specific information. This information is then analyzed to gain insights through artificial intelligence, enabling closed-loop bioelectronic medical devices such as smart insulin pumps, connected pacemakers, neurostimulators, and performance monitoring devices, among many others. However, connectivity to these devices through traditional wireless techniques typically results in (*a*) high communication power and (*b*) vulnerability to hacking, as the wireless signals can be picked up by a nearby eavesdropper (1). Evidently, the communication power consumed in a sensor node is usually orders of magnitude higher than the sensing and computation power (2, 3). However, a sensor node on, in, or around the human body does not need to communicate continuously because of data redundancy in either the temporal or spatial domain. Spatiotemporal in-sensor analytics (ISA), in the form of compressive sensing (CS),

anomaly detection, and collaborative intelligence, has recently been shown to reduce the communication power by orders of magnitude while losing less than 2% of information (4). ISA reduces the transmission payload of the sensor and thereby decreases the communication power, which, in turn, reduces the amount of power needed to sense and transmit a unit amount of information.

While ISA reduces the energy requirements of sparse information systems, other sensor nodes with continuous data streaming to the cloud require low-power communication, which is among the foremost requirements for connected biosensors as a result of their energy constraints. Another important consideration is information security (5, 6). With traditional wireless techniques like Bluetooth, an attacker could hack into a pacemaker, insulin pump, or brain implant simply by intercepting and analyzing the wireless signals. In reality, this has not yet happened, but researchers have been demonstrating the risks for more than a decade (1, 7).

Traditional wireless techniques use radiative communication among wearable and implantable devices using electromagnetic (EM) fields. Owing to the radiative nature of conventional wireless communication, EM signals propagate in all directions, which could inadvertently allow an eavesdropper to intercept the information. In this context, the human body, primarily due to its high water content, has emerged as a channel for low- to medium-loss transmission, enabling an energy-efficient means of data transfer termed human body communication (HBC). However, beyond the electro-quasistatic (EQS) range of frequencies (frequencies higher than a few tens of megahertz, where the wavelength becomes similar to the length of the human body and effectively makes the body a radiative antenna), conventional HBC implementations suffer from significant EM radiation, which also compromises security.

Secure, low-power communication techniques (such as EQS-HBC or MedRadio), along with spatiotemporal ISA and CS, have shown immense promise toward building a virtually zero-power, secure network of biomedical sensor nodes for applications including continuous monitoring, brain–machine interfaces, and closed-loop bioelectronic medicine. The extremely low power of EQS-HBC (8–10) enables perpetual wearable and implantable devices with simultaneous sensing, computation, communication, powering, and stimulation for myriad biosensors. A secure, low-power connectivity solution for multiple sensors on, around, or in the body is termed the Internet of Bodies (IoB) (11; see **https://engineering.purdue.edu/C-IoB**) (**Figure 1*a***). Various sensors on the body, such as blood pressure (BP), electrocardiogram (ECG), electroencephalogram (EEG), photoplethysmogram (PPG) and glucose sensors, collect information about different biophysical parameters. All of these sensor nodes need to have individual energy-harvesting, power management, ISA, and on-body communication modalities such that they either communicate among themselves or transmit the collected information to an on-body hub, such as a smartwatch. This on-body hub needs to have its own source of power, processing (edge analytics), local monitoring and control, network management, and a communication modality to transmit information to the cloud. The cloud performs central monitoring and control, and can send important information and control signals back to the on-body hub and the sensor nodes. The extent of resource availability (in terms of energy, memory, and processing capabilities) decreases from the cloud to the hub to the individual sensor nodes; therefore, the design of these sensor nodes is extremely important for both low overall power consumption and high information transfer for unit energy consumption.

2. CONNECTED BIOELECTRONIC SOLUTIONS: INTERNET OF BODIES

As a subset of the Internet of Things (IoT), the IoB represents a network of tiny devices on, in, or around the human body, comprising functions such as sensing, analytics, communication, actuation, powering, and harvesting. These nodes range from health care devices such as continuous

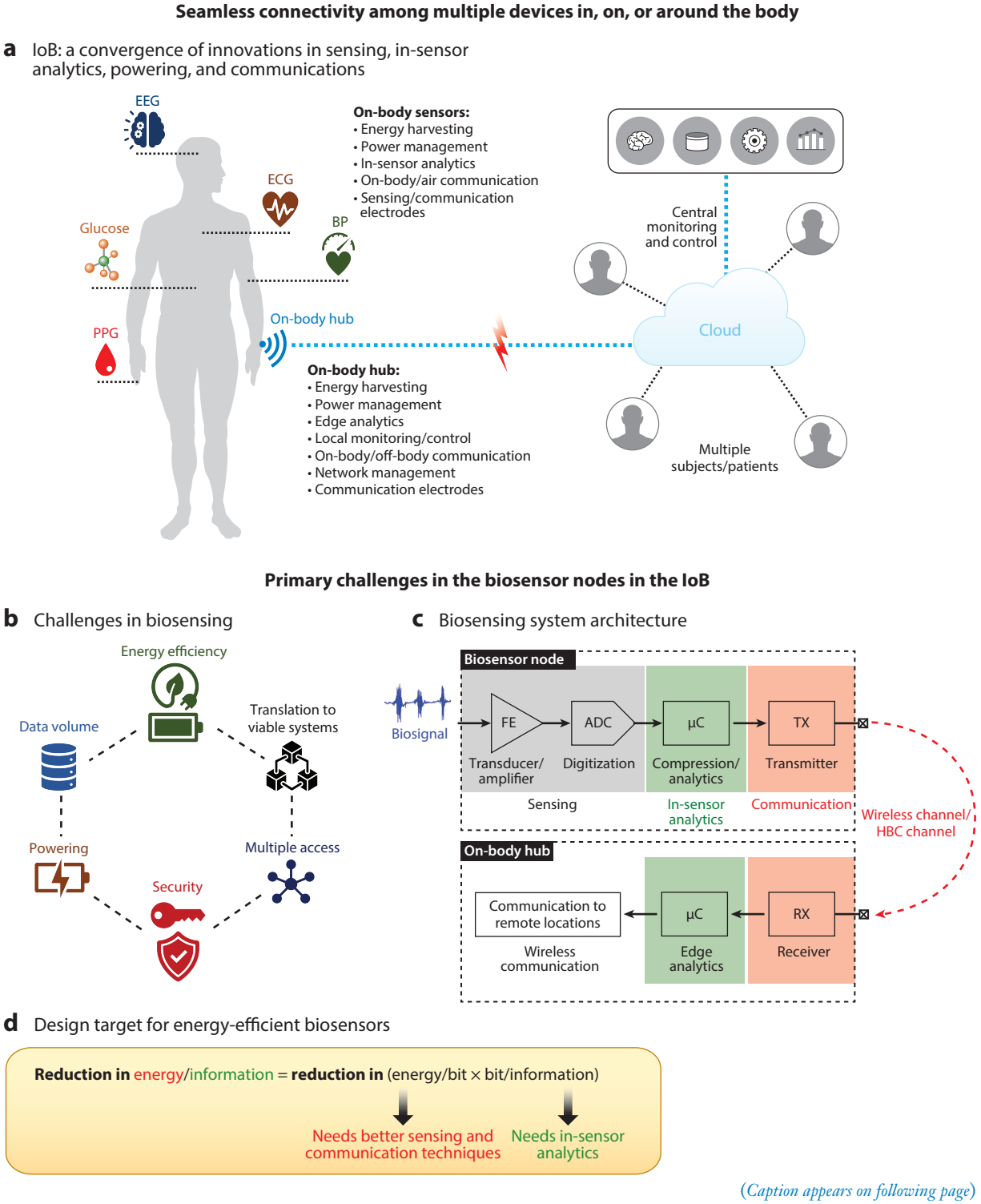

(*Caption appears on following page*)

Figure 1 (*Figure appears on preceding page*)

(*a*) The concept of the IoB and its applications in biosensing. (*b*) Six challenges in modern biosensing. (*c*) Example of a traditional biosensing architecture. (*d*) Design philosophy for energy-efficient biosensors. Abbreviations: ADC, analog-to-digital converter; BP, blood pressure; ECG, electrocardiogram; EEG, electroencephalogram; FE, front end; HBC, human body communication; IoB, Internet of Bodies; PPG, photoplethysmogram; RX, receiver; TX, transmitter; μC, microcontroller.

glucose monitors with connected insulin pumps, connected pacemakers, and ingestible pills to consumer electronic devices such as smartwatches, wireless ear pods, and augmented/virtual reality headsets. In the remainder of this review, we focus on the application of the IoB to connected bionodes and discuss various challenges and opportunities.

2.1. Challenges in Today's Connected Biosensors

The primary challenges in developing connected biosensors are shown in **Figure 1*b*** and discussed in the following subsections.

2.1.1. Energy efficiency. Wearable biosensors (on or around the human body) must operate with extremely low power consumption for extended battery life. For implanted devices, this requirement is even more stringent, as these devices need to operate either with harvested power (approximately tens to hundreds of microwatts) or with a cubic-millimeter-sized battery that can hold only ∼2 J of energy, assuming a state-of-the-art energy density of 2 kJ/cm^3 (see **https://en.wikipedia.org/wiki/Lithium-ion_battery**). As a result, even with an average power consumption of 10 μW, the battery will run out in less than 3 days, requiring that the patient undergo surgery to replace the battery. For this reason, the implanted bionode's power consumption must be lower than the limits posed by the various modes of energy harvesting.

2.1.2. Data volume. Modern biosensors can create huge volumes of data during continuous operation. For example, a single-channel neural sensor sampling neuronal activity (up to 10 kHz in frequency) at the Nyquist rate and with a 16-bit analog-to-digital converter (ADC) generates data at $10 \times 2 \times 16 = 320$ kbps. With 32 parallel channels, the bit rate increases to 10.24 Mbps, requiring extremely fast data transfer. Assuming that the data transfer occurs through traditional radio-frequency (RF) communication [which requires ∼1 nJ/bit (12)], the communication energy itself will exceed 10 mW, which is very hard to support with any form of harvested energy. Therefore, the data volume must be reduced through CS (13, 14), digital compression (9), or some other form of ISA.

2.1.3. Security. Small-form-factor biosensors have limited resources in individual nodes and thus can support only a subset of intended security features, such as software encryption. As a result, these devices are extremely prone to privacy attacks (15), so they require advanced design methodologies in which the security features are built into the hardware itself (i.e., hardware security) (16–19) and the hardware's physical properties enhance security (20, 21).

2.1.4. Powering. As explained in Section 2.1.1, powering of wearable or implantable biosensors poses significant challenges in terms of achievable energy consumption by the sensors and today's battery technology, requiring frequent battery replacement. Energy-harvesting techniques involving near-infrared (NIR) (22, 23), ultrasonic (24–29), thermoelectric (30), RF/inductive (31–33), magnetoelectric (34–36), capacitive (37–39), and human body–coupled EQS (9, 10, 40–44) modes of energy transfer have recently been investigated to solve the challenge of powering the biosensors. However, the highest possible harvested power that is achieved through these methods is usually ∼100 μW for reasonable form factors and channel lengths, leading to significant interest in development of sub–50 μW bionodes.

2.1.5. Multiple access. Another important consideration in developing a network of bionodes is the requirement for the channel (air for RF, the human body for HBC) to be accessed by multiple devices, which may operate at the same time or using the same frequency band. This capability may require (*a*) intelligent methods of frequency allocation when multiple devices access the channel at the same time, (*b*) duty cycling with separate communication slot allocations for multiple devices when they access the channel using the same frequency band, or (*c*) proper use of code-division multiple access when multiple devices access the channel using the same frequency band at the same time.

2.1.6. Network of nodes for multifunction operation. Multifunctional operation is another important requirement for future biosensing and actuation systems. For example, patients with certain neurological disorders can benefit from neuroprosthesis techniques to restore movement in paralyzed muscles. These systems traditionally focus on a single function with specific motor assistance, such as a hand grasp. However, paralysis often affects multiple aspects of life that patients want restored (45). Implementation of a separate system for each function is often impractical, since each device requires its own interface as well as real estate on the body. Additionally, heterogeneity across pathologies makes it difficult to use a single approach that is applicable to everyone. Therefore, a modular, scalable system that can be adapted to an individual's unique needs helps improve the patient's quality of life.

2.1.7. Translation of novel architectures to viable systems. In the past decade, a myriad of new circuits, architectures, and techniques have been proposed for bionode powering, sensing, and communication. However, translation of these techniques into viable systems that can be used for long-term monitoring is a major consideration that is often overlooked. Therefore, further research and evaluation are required to assess the practicality and safety of these techniques.

Figure 1*c* shows the traditional biosensing architecture, comprising a biosensor node and an on-body hub with which the biosensor node communicates. The biosensor node consists of a front end that amplifies and filters the incoming analog biophysical signal, followed by an ADC that digitizes the analog signal. A microcontroller can optionally be used for ISA; it performs some form of compression/analytics on the digitized data to reduce the volume of data to be communicated. Finally, a communication transmitter sends the data through a channel (which could be the wireless channel for EM communication or the human body itself for EQS-HBC), and the data are received by the on-body hub. In a biosensing scenario, the biosensor node is usually an extremely small wearable device or implant with limited resources (energy, memory, and computational power). In contrast, the on-body hub is expected to have greater resources due to the asymmetric network configuration.

The total amount of energy consumed in the bionode is given by Equation 1:

$$E_{\text{total}} = E_{\text{sensing}} + E_{\text{ISA}} + E_{\text{comm}}, \quad 1.$$

where

$$E_{\text{sensing}} = \text{bit}_{\text{sensed}} \times E/\text{bit}_{\text{sensing}}, \quad 2.$$

$$E_{\text{ISA}} = f\{\text{bit}_{\text{sensed}}\}, \quad 3.$$

and

$$E_{\text{comm}} = \text{bit}_{\text{communicated}} \times E/\text{bit}_{\text{communication}}. \quad 4.$$

For a biosensing system, the primary goal is to minimize the total energy, E_{total}, while maximizing the amount of information transmitted. Therefore, the design philosophy (**Figure 1*d***) for energy-efficient biosensors is usually based on reducing the energy consumption per unit amount

of information eventually transmitted. This goal can be achieved by either (*a*) reducing the energy per bit, which requires better sensing and communication techniques (discussed in Sections 3 and 4, respectively), or (*b*) reducing the number of bits per unit amount of information, which requires ISA (discussed in Section 5).

2.2. Societal and Medicinal Impact of Connected Biosensors: Wearable and Implantable Devices

Expenditure on wearable and implantable health care devices has become a significant portion of overall health care expenses in the USA. From 2018 to 2019, US health care costs increased by 4.6% to US$3.8 trillion, or 17.7% of gross domestic product (46). By 2023, these costs are projected to exceed US$5.1 trillion, of which more than 15% will be spent on wearable and implantable devices. These continuous monitoring systems are expected to improve at-home patient care and diagnostics, and electroceuticals (including neuromodulation techniques) will provide opportune and appropriate neurostimulation that promises to replace or augment pharmaceuticals.

2.3. Energy Requirements in Biosensor Nodes

The energy requirements of a biosensor are often dominated by the energy requirement for communication (2, 3). Assuming the energy efficiency of wireless communication is ∼1 nJ/bit (12), a transmitter would consume ∼1 mW power for a nominal data rate of 1 Mbps (the expected rate for a multichannel neural recorder, for example). Additionally, a traditional bionode includes an ADC for digitization and an optional CS unit for data volume reduction. Each of these modules would consume ∼50–100 μW power at the target data rates for state-of-the-art implementations (9, 47). Therefore, the overall power consumption of the transmitter would be ∼1.2 mW—more than three times higher than in the established energy-harvesting techniques for millimeter- to centimeter-scale implants. Consequently, achieving a reduction in communication power has attracted significant attention in recent years. A <50 pJ/bit (at 1 Mbps) wireless communication technique involving both MedRadio and HBC standards (48) renders the communication power similar to that of digitization and compression.

2.4. Achieving Ultralow-Power Biosensor Nodes

To achieve ultralow-power biosensing, all of the submodules in the bionode (sensing, computation/analytics, and communication) must incorporate certain innovations in terms of energy efficiencies. Furthermore, powering and network-level interaction techniques must be implemented so that the bionode can operate continuously without manual intervention.

2.4.1. Low-power sensing techniques. Low-power sensing techniques including CS, time-domain sensing, and collaborative sensing have garnered significant interest in recent years. CS utilizes the inherent sparsity of biophysical signals and reduces the digitized communication payload, thereby reducing communication energy. Time-domain sensing can achieve moderate resolution (12–18 bits) for biosensors without using complex voltage-mode or current-mode architecture. This is possible because most of the biophysical signals are low frequency (hertz to kilohertz range) and, thus, the availability of "time" can be used to average the noise and achieve a high signal-to-noise ratio (SNR), eventually resulting in high resolution. Methods related to CS and time-domain sensing are discussed in detail in Section 3.

2.4.2. In-sensor analytics for reducing communication power. ISA can reduce communication energy either by making the communication event driven or by compressing the sensed data (4). Event-driven communication enables nonuniform duty cycling during data transmission,

which reduces the overall communication energy without losing important information. Some ISA techniques applicable to biosensors are discussed in detail in Section 5.

2.4.3. Communication and powering. In most cases, traditional RF communication around the body consumes more than 1 nJ/bit, which places significant constraints on high-speed communication (>1 Mbps or more, requiring >1 mW power) because, in most cases, energy-harvesting techniques can provide only ~100 μW power. The challenge is even greater for implants: Replacing a battery requires surgery, so energy harvesting is the only viable option (49). Recent techniques in low-power communication are discussed in detail in Section 4, and powering techniques are described in Section 6. Earlier publications from several research groups in all of these different domains are cited in this review and summarized in **Table 1**.

3. ULTRALOW-POWER SENSING: TOWARD BATTERYLESS, PERPETUAL OPERATION

To minimize energy consumption per unit information, investigators will need to explore energy-efficient techniques for sensing and communication requirements, along with data volume reduction using ISA. This section discusses recent methods in energy-efficient sensing.

Table 1 Popular research directions for the constituent elements of biosensing nodes

	Modality/architecture	Salient features	References
Sensing	High-impedance, chopper-stabilized front ends	Low frequency, low noise	50–52
	Voltage- versus time-domain architecture	Low frequency, low power	56, 57
	Compressive sensing	Sparse signals, low power	58–61, 63, 66–68
	ADC-less sensing	Low frequency, extremely low power	69, 70
Communication	MedRadio/low-power wireless	Low interference, low power	48, 76, 89
	EQS capacitive HBC	Ultralow power, physically secure	75, 77–83
	EQS galvanic HBC and biphasic HBC	Short distance (few centimeters)	9, 70, 84
	MQS (magnetic) HBC	Approximately near field; no effect of body	85–87
	EM-wave HBC	High DR, good energy efficiency, not as secure	88
In-sensor analytics	Event-driven compression	Asynchronous, low power	60, 61
	Spike and/or anomaly detection	Asynchronous, ultralow power	97–103
	Learning-based analytics	Low power machine learning	111, 112
Wireless powering	Near-infrared	Lowest form factor, needs repeater	22, 23
	Ultrasound	Low form factor at low frequencies, needs repeater	24–29
	RF/inductive	Large coil/antenna, traditional architecture	31–33
	Magnetoelectric	Better power transfer efficiency than RF, safe	34–36
	Capacitive	Larger form factors, short distances	37–39
	EQS	Full-body powering for wearables	9, 40–42

Abbreviations: ADC, analog-to-digital converter; DR, data rate; EM, electromagnetic; EQS, electro-quasistatic; HBC, human body communication; MQS, magneto-quasistatic; RF, radio-frequency.

3.1. Biosensing Systems and Their Salient Features

Many naturally occurring biophysical signals, such as ECG, EEG, electromyogram, and electrocorticogram, are slowly varying. Most of the energy content of these signals is contained within low frequencies (1 Hz–10 kHz), as shown in **Figure 2*a*** (50). However, the resolution and dynamic range requirements for these applications can be large (12–16 bits for traditional biosensing

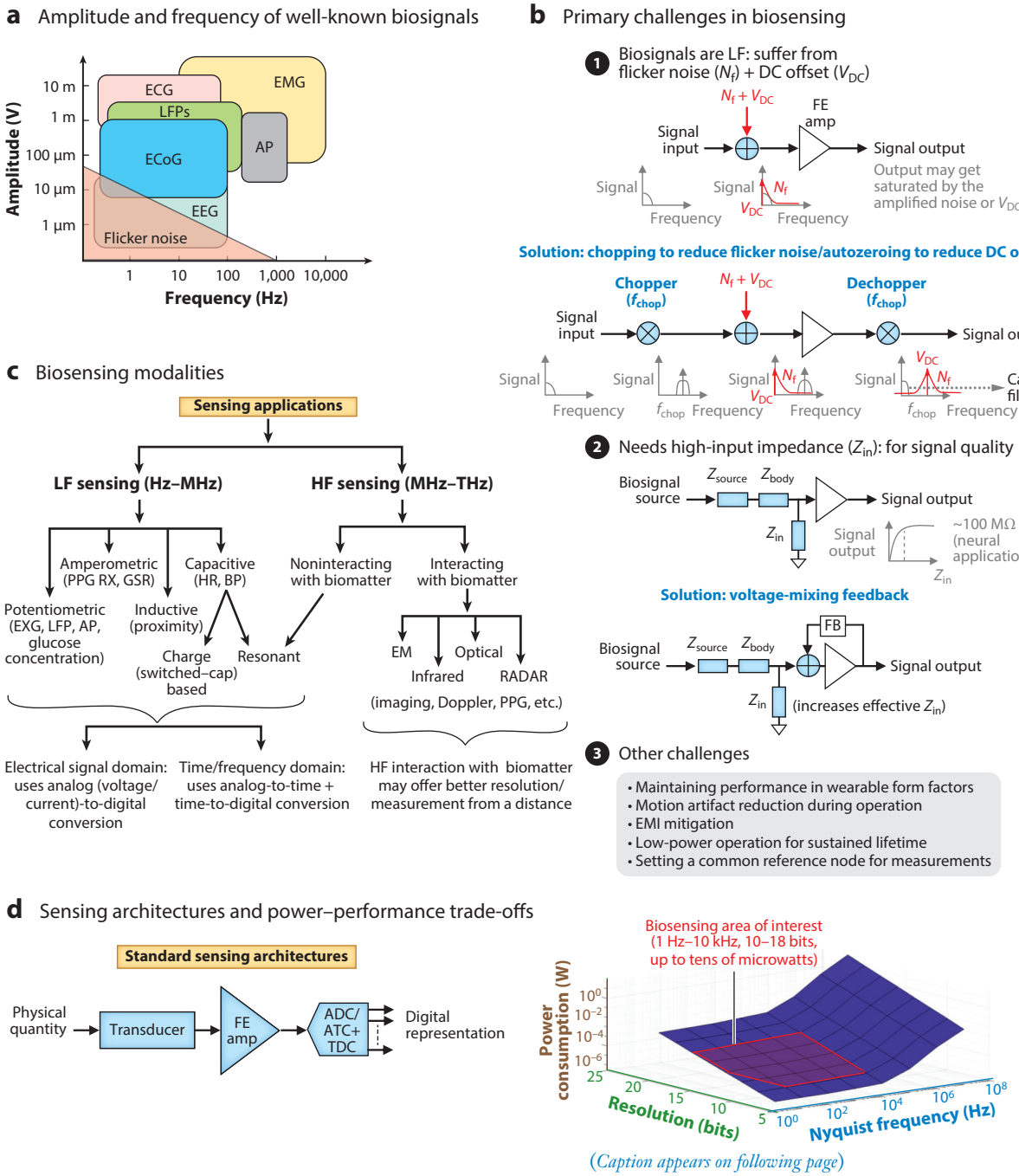

(Caption appears on following page)

Figure 2 (*Figure appears on preceding page*)

(*a*) Amplitudes and frequencies of well-known biosignals, indicating the requirement for LF (1 Hz–10 kHz) sensing of low-amplitude (up to microvolt) signals. (*b*) The primary challenges in such systems arise from LF flicker noise that coincides with the frequency of the biosignals and from requirements for high input impedance and high resolution. However, the power consumption of (*c*) different modalities and (*d*) architectures usually lies within a range of a few tens of microwatts. Abbreviations: ADC, analog-to-digital converter; AP, action potentials; ATC, analog-to-time converter; BP, blood pressure; ECG, electrocardiogram; ECoG, electrocorticogram; EM, electromagnetic; EMG, electromyogram; EMI, electromagnetic interference; EXG, collective term for ECG, ECoG, and EMG; FB, feedback; FE, front end; GSR, galvanic skin response; HF, high-frequency; HR, heart rate; LF, low-frequency; LFP, local field potentials; PPG, photoplethysmogram; RX, receiver; TDC, time-to-digital converter. Panel *a* adapted from Reference 50. Data in panel *d* from Reference 55.

applications and up to 20 bits for extremely low amplitude EEG). Traditional voltage-mode and current-mode ADC designs in such high-resolution applications become severely limited by the low-frequency flicker noise originating from the amplifiers and ADCs, as well as by requirements for high input impedance, low DC offsets, and low power consumption (**Figure 2*b***). Techniques such as chopping help mitigate the challenges posed by flicker noise. Flicker noise (or $1/f$ noise) arises from Si–SiO_2 interface nonidealities in traditional complementary metal-oxide semiconductor (CMOS)-based circuits (used to amplify and digitize biosignals) and is most prevalent at lower frequencies. Chopping upconverts the input biosignal to a higher frequency, so that the low-frequency flicker noise at the input of the CMOS amplifier does not affect the biosignal (51, 52). Similarly, autozeroing techniques or DC servo loops (51–53) help reduce any DC offsets resulting from the electrodes used for acquisition of the biosignal. Voltage-mixing/positive-feedback techniques help improve the input impedance of the sensor (52, 53), so that most of the signal is available at the input of the sensor.

The sensing itself can be divided into low-frequency (hertz–megahertz) and high-frequency (megahertz–terahertz) techniques (**Figure 2*c***). Low-frequency techniques can be potentiometric, amperometric, inductive, or capacitive, each of which can be read out either in the electrical signal domain (voltage/current) or using time-domain techniques (frequency/time period). High-frequency techniques can be either noninteracting with the biomatter (such as resonant techniques used to read out a capacitive sensor) or interacting with the biomatter (such as imaging, Doppler, or PPG systems). The interacting techniques offer better resolution and, sometimes, measurement from a distance (54). If we plot the power consumption of such sensing front ends with respect to ADC resolution and Nyquist frequency (55), we find that for the biosensing area of interest, the power consumption is usually limited to the range of a few to tens of microwatts, which is significantly lower than the commonly observed milliwatt power consumption of communication.

In recent years, time-based ADCs have attracted significant interest because of their ability to utilize the availability of time (since signals are of very low frequency) in an energy resolution–scalable manner (2, 56, 57). For high-resolution requirements, the signal to be sensed is converted into an equivalent frequency, and it is then simply observed using a counter for a longer amount of time for a change in the average frequency. For low-resolution requirements, the frequency is observed for a shorter amount of time and can then be turned off (through duty cycling) to save energy.

Even though time-based methods ensure energy resolution scalability within a certain range, the resolution cannot be made infinitely high by measuring for a longer time (or averaging the noise). The ambient noise statistics; process, voltage, and temperature variation; and jitter accumulation in the ring oscillator would limit the achievable resolution, of which jitter accumulation is the dominant factor (56, 57) in a controlled environment. The scaled quantization error in measuring a fixed frequency within a predefined amount of time decreases with the time of measurement. However, the accumulated jitter from the ring oscillator increases with the total time

of measurement. If the slope of the linear plot of accumulated jitter versus measurement time is k, then the achievable resolution is limited to $\log_2(1/k)$ bits.

3.2. Emerging Techniques in Ultralow-Power Sensing

Some of the emerging techniques that aim to minimize power consumption and/or the quantity of data generated are presented in the following subsections.

3.2.1. Compressive sensing. Compressed-domain sensing/CS (13, 14) is a mathematical tool in signal processing that defies the Shannon–Nyquist sampling theorem by sampling a sparse signal at a rate lower than the Nyquist rate while still being able to reconstruct the signal with negligible error. Since its inception, CS has been used in medical imaging (58), ISA (59), health care (60, 61), neural (9), and audio acquisition (62, 63) applications. CS algorithms assume that the signal to be sampled has a sparse representation, and sparse signals with randomly (i.e., from an independent and identically distributed Gaussian distribution) undersampled data can be recovered with low error by formulating them as an optimization problem. Therefore, the advantage of using CS is twofold: (*a*) CS allows a lower sampling rate, which reduces the power consumption in the ADC and clock generation circuitry, and (*b*) compression creates a smaller quantity of data with rich information content, which reduces the burden on the subsequent processing and communication modules.

Because many biophysical signals can be represented in sparse form (64), it is possible to leverage the superior energy efficiency of CS for biosensing (for two comprehensive reviews on CS, see References 64 and 65). One publication (66) used submicrowatt CS hardware employing 65 nm CMOS technology with online self-adaptivity for incoming signals with varying sparsity. Initial efforts toward self-adaptivity used either an asynchronous ADC with an adjustable sampling rate (67) or temporal decimation and wavelet shrinkage (68). Both techniques were utilized with specific incoming signals. Another, more general technique (66) exploits online sensory data statistics for dynamic reconfiguration (in terms of compression algorithm, compression harshness, and sampling frequency). Recent publications (9, 62, 63) have demonstrated a fully digital CS subsystem equipped with an on-chip, two-stage sparsifier and a dual varying-seed pseudorandom bit sequence sensing-matrix generator, with a variable compression factor ranging from 5 to 33.33. The two-stage discrete wavelet transform–based sparsifier ensures that the CS module works effectively for both sparse and nonsparse signals.

3.2.2. ADC-less sensing. Traditional sensor nodes consist of a transducer, analog amplifiers, an ADC, an optional digital compression unit, and a digital communication module. The ADC consumes a large amount of power while creating multiple bits from each sample of the input data, increasing the burden on the communication module. The digital compression unit reduces this communication burden by lowering the number of bits to be transmitted, but it consumes additional energy. An alternative is to use an ADC-less architecture, which creates a pulse width–modulated signal corresponding to each input sample. This process encodes the analog information into the analog pulse width of the signal, which can still be communicated using a digital-friendly transmitter, since the amplitude of the pulse width–modulated signal remains rail to rail. This method was proposed by Naderiparizi et al. (69), while Chatterjee et al. (70) reported the first integrated circuit implementation for resource-constrained wireless neural implants, obviating the need for power-hungry ADC and digital compression modules.

Given that all biosensing applications involve asymmetric resource distribution (the sensor nodes/transmitters usually have limited resources, while the hub/receiver can have greater resources in terms of energy, memory, and processing capabilities), reducing energy consumption at

the node transmitter through the use of such ADC-less architectures would be extremely useful. This area is one direction for future research.

3.2.3. Collaborative sensing. Collaborative wireless sensor networks (71, 72) can sense an analog signal from multiple sensors, utilizing collaborative efforts among the sensor nodes and their communication with one another and with the cloud. The power optimization and trade-offs of such networks have been analyzed (4) for large-area IoT test beds, and these networks can be used for biosensing applications as well.

The techniques described above help reduce the energy cost of sensing. However, energy consumption during communication is usually the dominant component of a biosensor node; for this reason, it is extremely important to choose a data transmission modality that helps reduce the overall, system-level power consumption.

4. ULTRALOW-POWER COMMUNICATION: DESIGNING PERPETUAL SYSTEMS

4.1. The Journey from Personal Area Networks to Body Area Networks to the Internet of Bodies

Communication in the IoB can be categorized in terms of the source of the data (which is the biosensing node) or the destination of the data (**Figure 3*a***). The destination could be any of the following:

- An on-sensor processor. The processor could be at a distance of a few millimeters to centimeters, and the communication may require only petajoules-per-bit energy, as wired communication can be used in this scenario.
- An on-body processor/aggregator. This device could be a smartwatch, for example, at a distance of a few centimeters to meters, and would require body area network (BAN)-based communication. Technologies available for this purpose include Bluetooth low-energy (BLE), Zigbee, ANT, MedRadio, HBC, and so forth, which can consume 10–1,000 pJ/bit of energy, depending on the design.
- A remote processor at an off-body access point. The processor could be at a distance of a few meters and would require a personal area network (PAN) for communication. Technologies available for this purpose include BLE, Zigbee, Wi-Fi, ANT, and so on, all of which could consume more than 1 nJ/bit of energy.

Most wireless communication techniques employed for BANs and PANs (for example, BLE, Zigbee, ANT, or Wi-Fi) typically consume two to three orders of magnitude more power than sensing and computation, making them the biggest bottleneck in achieving energy-harvested/batteryless sensor nodes (2, 3, 73, 74). For a megabit-per-second communication link, wireless data transfer results in power consumption of 1 mW or more (**Figure 3*b***). Note, however, that all biosensors will eventually be envisioned to perpetually operate using harvested energies from various (light, vibrational, thermal, RF, inductive, magnetic, human body–coupled) sources; these energies would be limited to a few hundred microwatts even in the most favorable conditions. Therefore, we need to either reduce the communication burden through better ISA techniques or decrease the number of petajoules per bit of the communication itself.

When research on low-power BANs started in the late 2000s, there was little difference between techniques used for BANs and PANs. However, with the widespread use of new and emerging techniques such as extremely low power MedRadio or HBC, the energy efficiencies in BAN communication decreased to ∼10 pJ/bit (48, 75). This decrease led to an ∼100-fold increase in power benefits over traditional wireless technology, bridging the gap between

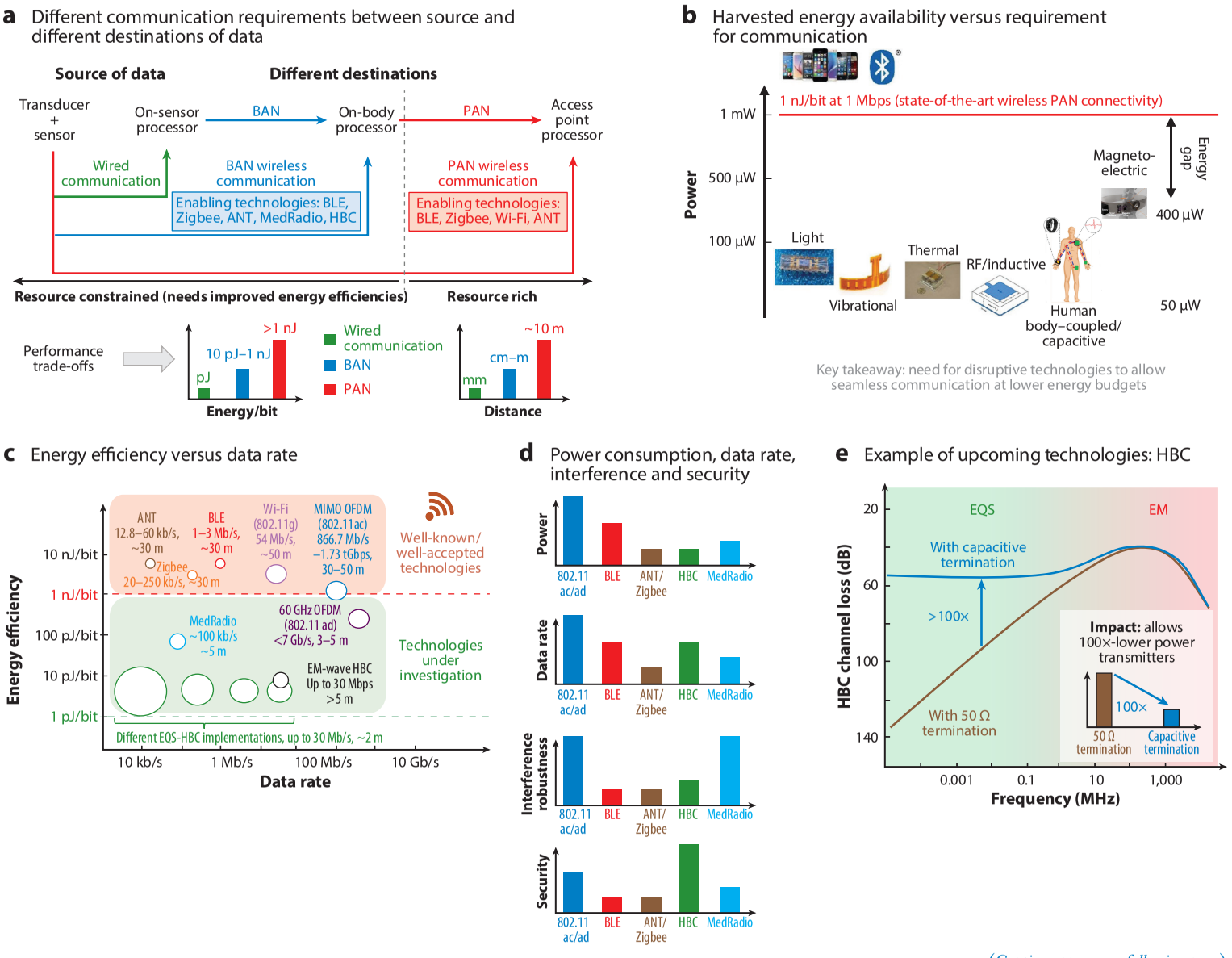

(Caption appears on following page)

Figure 3 (*Figure appears on preceding page*)

(*a*) Communication requirements and technologies used between the source and different destinations of data in the Internet of Bodies. (*b*) The gap between harvested energy and traditional wireless communication requirements (73). (*c*) Energy efficiency versus data rate for available technologies. The radius of each circle indicates the qualitative security of the communication scheme. (*d*) Comparison of available technologies in terms of their power consumption, data rate, interference rejection capabilities, and security. (*e*) Benefits of upcoming capacitively terminated HBC technologies. Abbreviations: BAN, body area network; BLE, Bluetooth low-energy; EM, electromagnetic; EQS, electro-quasistatic; HBC, human body communication; PAN, personal area network; RF, radio-frequency. Panel *b* adapted from Reference 73.

sensing/computation power and communication power. As a result, the design of extremely low power biosensor nodes will become a codesign problem among sensing, computing, and communication (and perhaps even security), instead of being limited only by communication power.

Figure 3*c* depicts energy efficiency versus data rate for various communication technologies. Almost all well-known, traditional wireless techniques consume more than 1 nJ/bit and offer low EM security because EM waves are present even at a distance of 5–10 m, making the signals susceptible to hacking (1, 7). Emerging techniques such as low-power MedRadio (48, 76), EQS-HBC (9, 10, 70, 75, 77–87), and EM-wave HBC (88) offer improved energy efficiencies because of their lower carrier frequencies; lower output power (MedRadio/EM-wave HBC); and non–50 Ω, high-impedance terminations (EQS/EM-wave HBC). Interestingly, EQS-HBC signals stay relatively constrained within the human body, offering better security than EM. The amount of leakage increases with frequency, though, which means that low-frequency EQS-HBC offers very high physical security. However, because the human body is susceptible to various environmental interference, operation of devices using these techniques is much less robust than for those using standardized techniques such as MedRadio or MIMO OFDM (multiple-input, multiple-output orthogonal frequency-division multiplexing; IEEE 802.11 ac/ad), which were designed for low interference.

Figure 3*d* compares and contrasts different communication techniques for biosensors. For example, it shows the benefits of EQS-HBC with capacitive termination as an alternative to radio wave–based wireless BAN, terminated with a 50 Ω antenna. In EQS communication, low-frequency (<1 MHz) electrical signals are communicated between two sensor nodes (transmitter and receiver) placed on the body, using the human body as a transmission channel. Capacitive termination at both transmitter and receiver renders channel loss a function of capacitive division (75), meaning that we have a flat-band channel, even at low frequencies, instead of a high-pass channel, which is common in 50 Ω HBC systems. The use of lower frequencies for operation, along with a wide bandwidth, leads to improved energy efficiencies for EQS-HBC. EQS communication also performs better in terms of physical security, as most of the signal is confined within the body. In terms of excitation and termination at the receiver and transmitter, the main quasistatic modalities are the capacitive (75, 77–83), galvanic (84), magnetic (85–87), and biphasic (9, 70) modalities.

4.2. Low-Power Techniques in Wireless Communication for the Internet of Bodies

The following subsections present a nonexhaustive list of recent techniques in wireless communication for the IoB.

4.2.1. Low-rate wireless personal area networks and body area networks. The LR-WPAN (low-rate wireless personal area network) is a technical standard that is maintained by the IEEE 802.15.4 Working Group (which started in 2003). It focuses on low-power wireless communication techniques using physical-layer, data link–layer, and network-layer optimizations. In contrast,

BANs evolved as part of the IEEE 802.15.6 standard (2011), which aims to provide the low-power features of the 802.15.4 standard while optimizing for short-range communication around the body.

4.2.2. MedRadio. MedRadio (the Medical Device Radiocommunications Service, formerly called the Medical Implant Communication Service) aims to support the development of low-cost medical sensor technologies for diagnostic, therapeutic, and monitoring purposes by dedicating certain low-interference frequency bands (primarily near 400 MHz, although 2.36–2.39 GHz medical BAN devices also fall into the MedRadio category). The standards governing these technologies were developed in the late 1990s and early 2010s, when they became part of IEEE 802.15.6. However, with recent trends in low-power wireless integrated circuit design due to digital-friendly, high-speed, low-power processes, the MedRadio space has attracted renewed interest (48, 76, 89).

4.2.3. Human body communication. HBC uses the conductive properties of human tissue to communicate signals for devices located in, on, or around the human body. The use of low-frequency EQS signaling helps restrict the signals to the body, without significant leakage, while simultaneously achieving low power consumption due to the use of low carrier frequencies.

4.3. Emerging Techniques in Energy-Efficient Human Body Communication

In the next subsection, we discuss some of the emerging techniques in low-power/energy-efficient HBC.

4.3.1. Capacitively terminated, broadband, low-frequency electro-quasistatic human body communication. Use of the human body as a low-loss broadband communication medium (79, 80) enables energy efficiencies below 10 pJ/bit, similar to those of wireline transceivers (90, 91), as well as strong physical security (1). Maity et al. (75) were the first to create a sub–10 pJ/bit capacitive HBC link with voltage-mode signaling and high-impedance termination allowing broadband communication. The low channel loss and absence of up- or downconversion resulted in radically improved energy efficiencies.

The key challenge in broadband HBC comes from the antenna effect in the human body, which picks up unwanted interference that corrupts the signal. An interference detection and rejection loop using an adaptive notch at the integrating receiver enabled a 6.3 pJ/bit transceiver for 30 Mbps data transfer through the body (the energy efficiency was ∼100 times lower than that of traditional wireless BANs) with an interference-robust (i.e., able to tolerate a −30 dB SNR) HBC transceiver. Chatterjee et al. (48) and Park & Mercier (86) later developed <10 pJ/bit transceivers with on-chip clocking architectures. For ultralow-power physiological monitoring and secure authentication, Maity et al. (8) recently demonstrated a 415 nW capacitive EQS-HBC link with data rates of 1–10 kbps that exhibits physical and mathematical security through integration of an AES-256 encryption engine with the HBC transceiver. Chatterjee et al. (83) analyzed the theoretical limits of power consumption in such systems and demonstrated adiabatic techniques with a hardware-aware modulation scheme to improve energy efficiencies. In the future, such low power levels could enable the design of batteryless wearable patches.

4.3.2. Multimode resonant human body communication for communication and powering. A major source of power consumption in a voltage-mode capacitive HBC transmitter is the interelectrode parasitic capacitance. The use of an inductance across this capacitor presents a parallel resonance at the load of the transmitter, which in turn reduces power consumption during data communication (40–42). Similarly, the use of a series resonance at the transmitter output

(with a series inductor) increases the output voltage by a factor of Q (where Q is the quality factor of the inductor). Because the power transfer in a voltage-mode capacitive HBC link increases quadratically with the output voltage of the power transmitter, this method increases the power transferred through the body by a factor of Q^2. In comparison to two studies (40, 41) in which the amount of power transferred decreased with distance between the transmitter and receiver, a third study (42) achieved almost constant power transfer and efficiency throughout the body because the operation was at a much lower frequency [1 MHz (42) versus 40 MHz (40, 41)].

4.3.3. Biphasic quasistatic brain communication for powering and communicating with deep brain implants. Capacitive HBC is not very effective in implantable devices because of the absence of a strong return path from within the body. In contrast, galvanic HBC consumes more power because a significant amount of DC current flows into the surrounding tissue if the signal is not DC balanced. Biphasic QBC (9) reduces power consumption in the galvanic modality by using AC coupling at the output. In comparison to galvanic HBC, biphasic QBC achieves ~41 times less power at an EQS frequency of 1 MHz.

Even with such low-power data communication techniques, the energy cost of communication still dominates in a biosensor node. Consequently, it is imperative to investigate available in-sensor computation techniques that can reduce the computation burden in the node.

5. IN-SENSOR DATA ANALYTICS: COMPUTATION VERSUS COMMUNICATION

As the number of distributed sensors in the IoB increases, the total amount of data transfer to the back-end hub/cloud servers becomes prohibitively large, resulting in network congestion and high energy consumption during data transmission at the sensor node (92). This motivates the need for ISA, which can perform context-aware data acquisition with some amount of computation, followed by transmission if necessary, resulting in interesting trade-offs (**Figure 4*a***). Depending on the amount of ISA performed in the biosensor, the total energy could be dominated by either the communication energy or the computation energy.

5.1. Trade-Offs Between Computation and Communication

The computation and communication energies (E_{comp} and E_{comm}, respectively) in a biosensor node are defined as follows:

$$E_{comp} = (E_{comp}/\text{bit}) \times \text{number of bits switched}, \quad 5.$$

$$E_{comm} = (E_{comm}/\text{bit}) \times \text{number of bits transmitted}. \quad 6.$$

For digital computation units (which are the conventional implementation), the low-frequency region of E_{comp}/bit is usually dominated by the static leakage current in the devices used for computation, while the high-frequency region is dominated by the dynamic energy of bit switching (93, 94). For optimum energy efficiency, the designer looks for a region where the sum of the leakage and dynamic energies can be minimized. As a result, E_{comp}/bit is in the range of a few femtojoules to petajoules. On the other hand, E_{comm}/bit is usually determined by the receiver's bit error rate sensitivity for a particular data rate, by the communication channel loss, and by the transmitter's efficiency (2, 4). As a result, E_{comm}/bit typically ranges from hundreds of petajoules to a few nanojoules for modern implementations.

Figure 4*b* compares E_{comm} with E_{comp} for the same number of bits being computed or communicated. State-of-the-art wireless transceiver implementations (95) consume ~10^4 times more

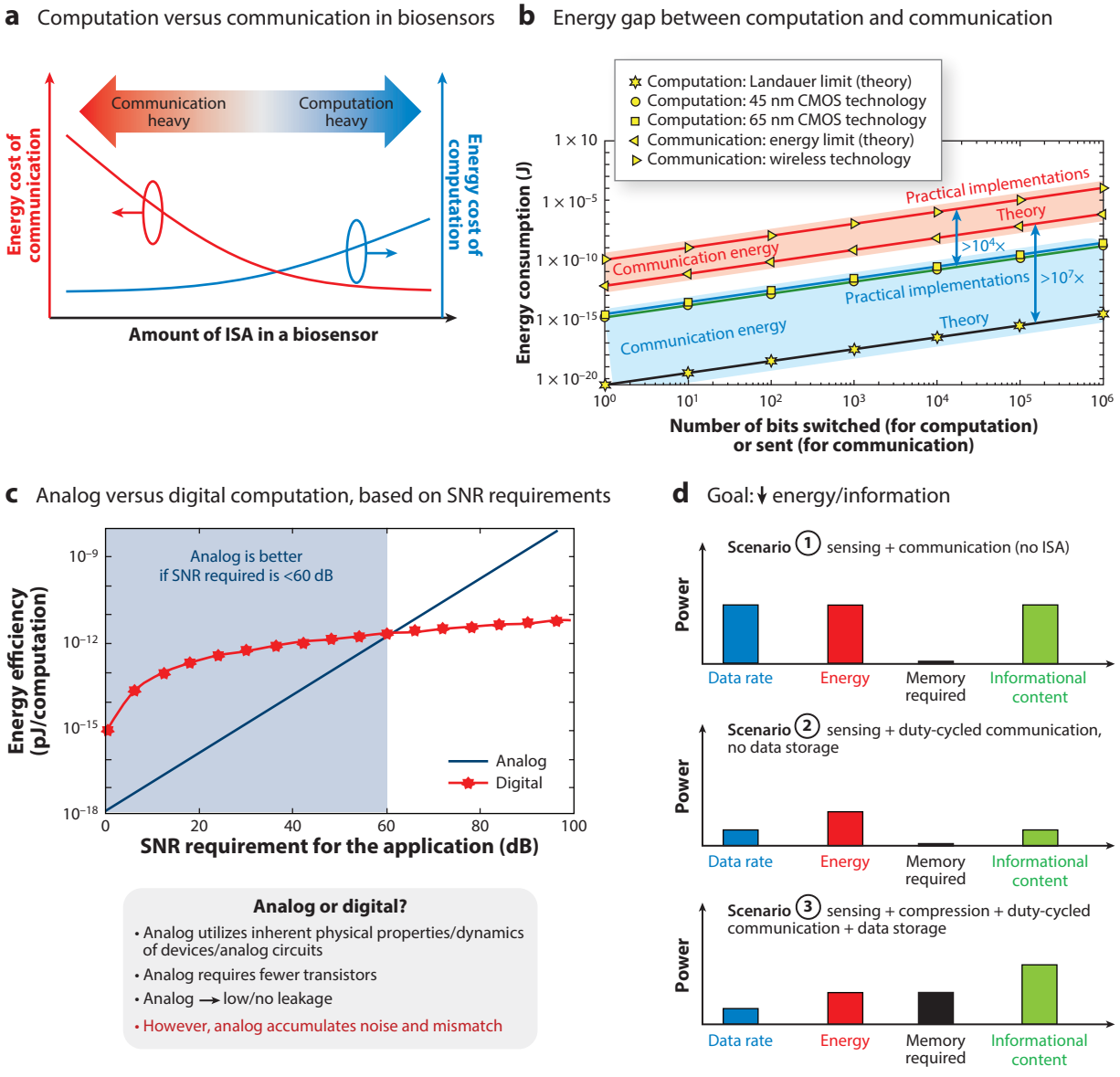

Figure 4

(*a*) Computation versus communication energies in a biosensor, based on the amount of ISA performed. (*b*) Comparison of communication and computation energies [both theoretical and from standard implementations (2)], showing that communication energy is ~10^4 times higher than computation energy (with the same number of bits). (*c*) Trade-offs between analog and digital computation (96). (*d*) Trade-offs in scenarios involving (①) no ISA, (②) duty-cycled communication, and (③) compression with duty-cycled communication. Abbreviations: CMOS, complementary metal-oxide semiconductor; ISA, in-sensor analytics; SNR, signal-to-noise ratio. Figure adapted with permission from References 2 and 3.

energy than computational bit switching in 45 nm and 65 nm technology nodes. This bottleneck analysis signifies that intelligent computation within a sensor node (ISA) can reduce total energy consumption by enabling selective data transmission, which decreases E_{comm} at the cost of additional E_{comp}.

Figure 4*c* shows the trade-offs involved in implementing an analog versus a digital computation unit in terms of the SNR requirement of the application (96). For low-SNR requirements, an analog unit can perform much more power-efficient computations due to the use of inherent device properties for computation (for example, vector multiplication of transconductance with input voltage can generate a vector output current, and Kirchhoff's current law can help add those vector currents, without any bulky digital multiplier or adder). The analog implementation also leads to fewer devices, resulting in lower power. However, analog units suffer from accumulation of the effects of noise and mismatch over multiple stages, so they are beneficial only for applications that can tolerate low SNR.

Finally, **Figure 4*d*** shows the trade-offs in three different scenarios. In the first scenario, no ISA is considered, and the sensed data are simply transmitted out using continuous streaming, leading to a high amount of power. In the second scenario, the communication is duty cycled, resulting in lower data rates and lower power but also lower information content. However, in the third scenario, by enabling compression and in-sensor storage, we can send more effective information per unit amount of power, at the cost of additional memory requirements.

5.2. Examples of In-Sensor Analytics in Biosensing

On the basis of the communication and computation energy trade-offs, the application at hand, and the amount of resources available at the resource-constrained biosensor node, partial or complete processing of the acquired data can take place in the sensor node itself [for example, spike timing detection compression for an implanted neural node (97–99)]. In this section, we discuss some common ISA techniques for biosensors, including anomaly/outlier detection and data compression, spike detection and spiking band power calculation for neural sensors, and machine learning–based analytics.

5.2.1. Anomaly detection and data compression. Anomaly detection methods can enable selective (and immediate) data transmission when an anomaly occurs in an otherwise normal sensor readout. For example, in health care, selective ECG data transmission with arrhythmia (anomaly) detection would ensure immediate notification with minimum communication cost. Data compression, on the other hand, would ensure that the maximum quantity of information between transmissions can be stored in a small amount of on-sensor memory. Zhang et al. (60) used a matrix-multiplying ADC in 130 nm CMOS technology, demonstrating ECG-based cardiac arrhythmia detection. Anvesha et al. (61) demonstrated arrhythmia detection with a time-based CS ADC.

5.2.2. Spike detection for neural sensing. Researchers investigating neural signal acquisition applications have focused primarily on increasing the number of recording channels. As the number of channels increases, the quantity of data recorded increases, and it becomes infeasible to communicate all the data from a neural implant to a nearby hub. However, most of the information in the neural signals resides in the spikes; therefore, detecting and communicating the occurrence and shape of the spikes are enough for most applications. Detection of spike occurrence is typically performed by traditional thresholding methods. Although the shape of the spike is not preserved, simple thresholding is still useful in scenarios where only the occurrence of spikes is of interest (100, 101).

Various implementations of thresholding for spike detection have been reported (102, 103). Compression techniques have also been demonstrated on neural spikes using optimized vector quantization methods (104), CS (105–107), wavelet transform (108, 109), Walsh–Hadamard transform (98), and spiking band power calculation (99, 110). Wavelet transform– and

Walsh–Hadamard transform–based techniques retain information on both the occurrence and the shape of the spike.

5.2.3. Learning-based analytics. For wearable devices, in which the bionodes have greater resources than in implantable devices, lightweight machine learning algorithms (tinyML) can be implemented as a part of the data analytics. The algorithm in a transfer learning–based cuffless BP estimation technique using PPG (111) employs visibility graphs to create images from PPG signals with features related to the waveform morphology. The results demonstrate that the difference between the estimated and actual systolic and diastolic BP is -0.080 ± 10.097 mm Hg and 0.057 ± 4.814 mm Hg, respectively. This research has been extended to a small-scale convolutional neural network using a modified LeNet-5 architecture (112).

The research described in this section reinforces the need to incorporate certain processing capabilities into biosensor nodes according to their application. There will be interesting trade-offs among sensing, processing, and communication, which will differ according to the application and the particular modalities chosen for these three functions. However, these trade-offs will be governed by the devices' energy availability. In the next section, we discuss the various techniques for powering these nodes.

6. POWERING THE BIOSENSORS: ENERGY HARVESTING IN A WEARABLE OR IMPLANTABLE DEVICE

In the last decade, researchers have explored various modalities of bionode energy harvesting, including mechanical (vibrational, triboelectric, and piezoelectric), thermal (thermoelectric), radiative (photovoltaic, infrared, NIR, RF), chemical (electrochemical), magnetic (inductive and magnetoelectric), and electric (EQS-HBC and capacitive) methods. **Figure 5*a*** depicts the power densities for these techniques.

In comparison to wearable biosensors, the requirements for implanted biosensors are much more stringent as a result of the small form factor and lower amount of resources. Techniques including NIR light (22, 23), ultrasound (24–29), RF/inductive (31–33), magnetoelectric (34–36), capacitive (37–39), and EQS-HBC (9, 40–42) modes have recently been demonstrated.

Figure 5*b*,*c* shows the various modalities of powering an implant. The figure also compares these modalities in terms of parameters including the amount of tissue absorption/scattering, maximum power transferred, transduction efficiency, form factor of the device, robustness, and safety. RF/inductive methods suffer from tissue absorption, while ultrasound suffers from bone absorption (for example, in the skull for a brain implant). Hence, ultrasound methods require repeaters below the bone layer. Similarly, NIR requires repeaters to improve both powering and communication. Magnetoelectric methods exhibit extremely low loss within human tissues, since the human body has a relative permeability of ~1 at or below frequencies of tens of megahertz. As a result, magnetoelectric methods are safer than EM or EQS methods, and high magnetic fields can be applied across the human body so that the bionodes receive enough power. However, creation of such magnetic fields requires significant energy, which is somewhat acceptable given that the magnetic fields are created from the body-worn hub, which has higher energy resources. Capacitive and EQS-HBC methods do not suffer from significant tissue absorption or transduction losses. However, the capacitive mode of powering requires parallel conductive plates to be placed on either side of the tissue (creating a capacitor), which could increase the form factor of the device. EQS-HBC methods, on the other hand, rely on the creation of electric fields from the implant (bionode) to the hub; the signals pass through the tissue following the equations for dipole coupling (9, 10), thereby reducing the voltage received as a function of the distance squared.

a Energy availability of different modes of power transfer with a cm^3 volume

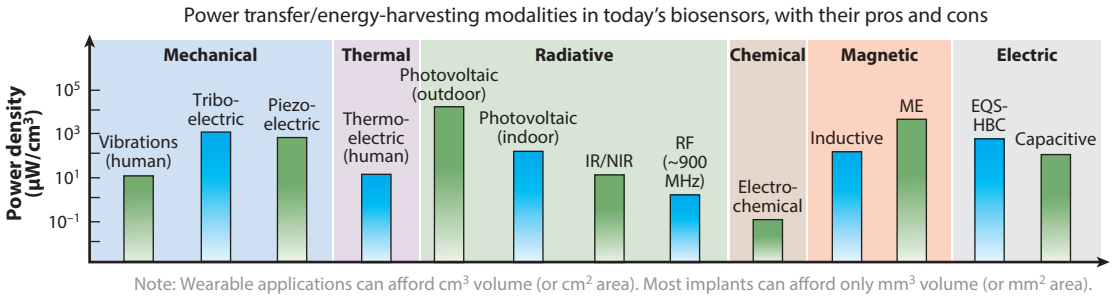

b Different methods of wireless power transfer to an implant (where certain modes such as photovoltaic or thermal gradients do not work)

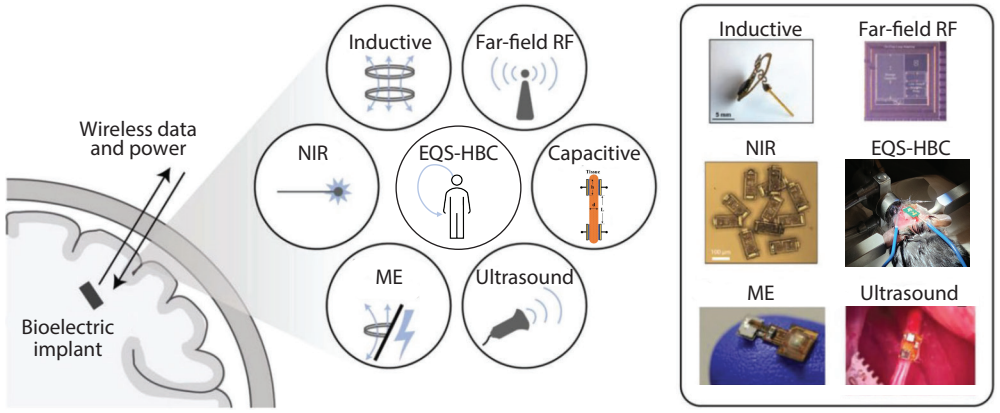

c Performance of different techniques for wirelessly powering an implant

Method	RF	Inductive	Ultrasound	NIR	ME	Capacitive	EQS-HBC
Tissue/bone absorption/scattering							
Maximum power transferred shown							
Transduction efficiency							
Device form factor							
Robustness							
Safety							

Best
Worst

Figure 5

(*a*) Available modalities of power transfer to a biosensor and their typical power densities. (*b*) A subset of modalities for powering an implant (49). (*c*) Comparison of power transfer modalities for an implant. Abbreviations: EQS, electro-quasistatic; HBC, human body communication; IR, infrared; ME, magnetoelectric; NIR, near-infrared; RF, radio-frequency. Panel *b* adapted from Reference 49.

6.1. Upcoming Methods of Powering a Wearable Device

Power transfer using RF/inductive methods has traditionally been employed for wearable nodes. Although the amount of power transferred using these methods can be hundreds of microwatts or more for a centimeter-scale device, there are certain limitations related to the device's form factors and the frequency to be used. Also, near-field power transfer is limited by distance, and

far-field methods suffer from body-shadowing effects (41). Additionally, the orientation of the inductive coils at the transmitter and receiver determines the amount of power transferred. Newer techniques for sending power through the human body (40–42) can transfer power throughout the body (and any wearable device, placed anywhere on the body, can pick it up) with no dependence on orientation.

6.1.1. Electro-quasistatic body-coupled powering. The first EQS powering techniques (40, 41) showed that body-coupled power transmission exhibits a path loss that is 30–70 dB lower than in far-field RF in the presence of body shadowing. The wearable system works with an operating frequency of 40 MHz and could recover 2 μW from a 1.2 mW source placed 160 cm away on the body. However, the amount of power transferred decreases with distance.

6.1.2. Resonant whole-body powering. Modak et al. (42, 43) reported a resonant whole-body powering technique that uses frequencies around 1 MHz, allowing similar path loss throughout the body (a better EQS scenario). Measurements showed a wearable–wearable power transfer of more than 5 μW from an ∼60 μW source (∼8% efficiency), regardless of where the device was located on the body. The system also employed a 2.19 μW communication system using EQS-HBC, which demonstrated the feasibility of communication with the harvested energy.

Cho et al. (44) recently developed an electrical model of on-body powering. They showed that more than 1 mW of power can be transmitted in favorable scenarios, including large devices and short distances.

6.2. Upcoming Methods of Powering an Implantable Device

The energy requirements for an implant are much more constrained than for a wearable device because of the implant's small size and the inability to use or replace batteries. RF, inductive, ultrasound, and optical methods of powering an implant suffers a high amount of end-to-end loss (for example, RF is absorbed in the tissue, while ultrasound is absorbed in the bones); therefore, repeaters are often required for both powering and communication. New capacitive, biphasic EQS, and magnetoelectric methods show promise in terms of device form factors, low amount of tissue absorption, and safety.

6.2.1. Capacitive powering. Capacitive powering techniques rely on power transfer using two sets of differential plates: One set of plates is part of the implant, while the other set is wearable (37–39). With capacitive patches measuring 20 mm long × 20 mm wide × 3 mm thick, and a 3-mm-thick beef tissue sample in between, the maximum amount of power transfer is 12 mW, with 36% efficiency (39). However, this method requires large capacitive plates and a short distance between the implant and the surface of the body.

6.2.2. Biphasic quasistatic brain communication. Chatterjee et al. (9) demonstrated the biphasic mode of powering along with communication. A headphone-shaped body-worn hub can send power to implanted neural nodes through differential excitation and pickup. A maximum of a few microwatts of power is available at an implant located 55 mm inside the brain with >35 V (root mean square) applied via the wearable hub. This method has low loss and avoids signal transduction, resulting in high end-to-end efficiency. However, it relies on the creation of large electric fields around the body for powering, which could give rise to safety concerns.

6.2.3. Magnetoelectric powering. Using the airlike permeability of the human body, magnetic fields can propagate through tissue with almost no loss. Researchers have used this property (34–36) to demonstrate ∼400 μW of power transfer to an implant from a wearable device that creates a 0.1 mT magnetic field at a distance of ∼30 mm. For isoenergy density, this magnetic field is

equivalent to a 300 kV/m electric field, which means that the creation of such magnetic fields will consume significant energy. However, the high power may be justified because the magnetic field is created at a wearable hub, with access to better power sources.

On the basis of the discussion presented in Sections 4–6, we believe that EQS-HBC/capacitive modes for communication and magnetoelectric methods for powering could become an optimum solution for small implants such as wireless neural nodes. For wearable applications, on the other hand, body-coupled powering and HBC show excellent potential for the development of extremely energy efficient, perpetual biosensor nodes.

7. A NOTE ON SECURITY AND DATA PRIVACY

Because of the resource constraints inherent in a small-form-factor bionode, advanced encryption techniques and high-overhead countermeasures for advanced attacks [such as side-channel attacks (SCA)] are often infeasible to implement on sensor nodes. However, standard encryption algorithms such as AES-256 can consume less than 200 nW power for data rates below 20 kbps (8) on a wearable sensor node.

7.1. Threat Models

Some of the most important threat models for biosensors are described in the following subsections.

7.1.1. Side-channel attacks. Even though the mathematical complexity of the key recovery algorithm for AES-256 is 2^{256} (which means that a brute-force method could break the encryption with a probability of $1/2^{256}$), nontraditional techniques such as EM SCA or power SCA can reduce the recovery complexity to only 2^{13}, which can be broken within 50 s (113). Correlational power analysis algorithms are used to break the AES key by looking at the fluctuations at the power lines during encryption; therefore, these algorithms pose less of a risk for wearable and implantable devices, as the attacker needs physical access to the devices. On the other hand, correlational EM analysis (CEMA) can break the AES key by analyzing the EM radiation from the devices during encryption. CEMA-based SCA pose a greater risk for biosensor security, as attacks can be performed even from a distance by use of a high-sensitivity receiver.

7.1.2. Replay attack/mimicking a device. A malicious attacker can impersonate a sensor node and replay/mimic the data transmitted by the original device, creating confusion at the receiver. If the malicious device transmits the data with enough power, it can also jam the intended transmission, resulting in loss of important biophysical information.

7.2. Hardware Solutions

Software-based masking techniques to prevent SCA require significant computational power. Therefore, we focus on low-overhead hardware solutions for both SCA and replay attacks.

7.2.1. Side-channel attack countermeasures. Das et al. (16) demonstrated a white-box modeling and signature attenuation countermeasure for EM and power SCA. This countermeasure is based on techniques such as current-domain signature attenuation (CDSA) (17, 18, 114) that help reduce the signatures used in power SCA, along with local EM signature suppression through low-level metal routing (18, 19).

CDSA uses a constant current source to supply the AES current, reducing the correlated fluctuations on the power lines during encryption and improving the figure of merit for correlational power analysis countermeasures. In contrast, local EM signature suppression is implemented by

routing the encryption hardware (the crypto engine) using lower-level metals in a CMOS process. This technique ensures that the higher-level, thicker metals in the CMOS process do not carry correlated currents during encryption, which could otherwise leak critical information in the form of EM signals. The use of these techniques led to a >33-fold SCA security improvement over the state of the art (18). A digital-friendly implementation of CDSA with low-level metal routing for fast time-to-market applications has been demonstrated (115).

7.2.2. Countermeasures against data mimicking. Physically unclonable function–based techniques are used to generate a device-specific signature, exploiting the inherent manufacturing process variations. However, these techniques are usually applied in the digital domain, which requires additional hardware and processing steps. Chatterjee et al. (20) proposed a new type of physically unclonable function for resource-constrained IoT and biosensor nodes that utilizes the analog and RF properties intrinsic to all transmitter nodes. Each transmitter inherently possesses analog/RF nonidealities on top of an intended digital signal (or the mimicked digital data, in the case of a malicious device) due to certain variations in the manufacturing process. Given that these nonidealities differ for every transmitter, in situ machine learning hardware at the resource-rich receiver can detect a particular transmitter by analyzing these nonidealities. A malicious transmitter that mimics (or alters) someone else's data can also be identified separately from the intended transmitter. The development of this system was motivated by the unique voice signatures in human-to-human communication, which our brains use to map a person's identity to their voice.

Undoubtedly, there is a strong demand for the incorporation of security features during design time for resource-constrained, small biosensor nodes to protect personal and health-related information, emphasizing the need for further exploration of low-cost, lightweight hardware security primitives. As a result, this area is quickly becoming a major focus of research in biosensors.

8. CONCLUSION: VISION FOR THE FUTURE

Biosensors differ from traditional wireless sensor networks in terms of specific challenges in wearable and implantable applications, including resource (energy, computation, memory) availability, security, and powering. In this review, we have identified the primary design objective of such connected biosensor nodes, which is to minimize the energy consumption per unit amount of information. We have focused on a broad analysis of the constituent units of such sensors in terms of sensing, processing, communication, and powering, all of which need to be designed for holistic, system-level resource optimization for constrained biosensors. We have also discussed numerous challenges in the form of system-level adaptive control, reliability, security, latency, and powering limitations, indicating future research directions toward smart, secure, and connected bioelectronic medicine, as well as the IoB in general, that has the potential to enrich human lives by leveraging progress in the various technologies discussed throughout this review.

DISCLOSURE STATEMENT

The authors are not aware of any affiliations, memberships, funding, or financial holdings that might be perceived as affecting the objectivity of this review.

ACKNOWLEDGMENTS

The writing of this review was supported in part by a National Science Foundation Career Award (grant 1944602) and by the Center for the Internet of Bodies (C-IoB).

LITERATURE CITED

1. Das D, Maity S, Chatterjee B, Sen S. 2019. Enabling covert body area network using electro-quasistatic human body communication. *Sci. Rep.* 9:4160
2. Chatterjee B, Cao N, Raychowdhury A, Sen S. 2019. Context-aware intelligence in resource-constrained IoT nodes: opportunities and challenges. *IEEE Des. Test* 36(2):7–40
3. Cao N, Chatterjee B, Gong M, Chang M, Sen S, Raychowdhury A. 2020. A 65 nm image processing SoC supporting multiple DNN models and real-time computation-communication trade-off via actor-critical neuro-controller. In *2020 IEEE Symposium on VLSI Circuits*, pp. 1–2. Piscataway, NJ: IEEE
4. Chatterjee B, Seo DH, Chakraborty S, Avlani S, Jiang X, et al. 2021. Context-aware collaborative intelligence with spatio-temporal in-sensor analytics for efficient communication in a large-area IoT testbed. *IEEE Internet Things J.* 8(8):6800–14
5. US Cybersecur. Infrastruct. Secur. Agency. 2019. *Medtronic Conexus radio frequency telemetry protocol* (*update C*). ICS Med. Advis. 19-080-01, April 8. **https://us-cert.cisa.gov/ics/advisories/ICSMA-19-080-01**
6. Waltz E. 2019. Can "Internet-of-Body" thwart cyber attacks on implanted medical devices? *IEEE Spectrum Blog*, March 28. **https://spectrum.ieee.org/thwart-cyber-attacks-on-implanted-medical-devices**
7. Sen S, Maity S, Das D. 2020. The body is the network: To safeguard sensitive data, turn flesh and tissue into a secure wireless channel. *IEEE Spectr.* 57(12):44–49
8. Maity S, Modak N, Yang D, Nath M, Avlani S, et al. 2021. Sub-μWRComm: 415-nW 1–10-kb/s physically and mathematically secure electro-quasi-static HBC node for authentication and medical applications. *IEEE J. Solid-State Circuits* 56(3):788–802
9. Chatterjee B, Gaurav K, Nath M, Xiao S, Modak N, et al. 2021. A 1.15 μW 5.54 mm^3 implant with a bidirectional neural sensor and stimulator SoC utilizing bi-phasic quasi-static brain communication achieving 6 kbps–10 Mbps uplink with compressive sensing and RO-PUF based collision avoidance. In *2021 IEEE Symposium on VLSI Circuits*, pp. 1–2. Piscataway, NJ: IEEE
10. Chatterjee B, Nath M, Gaurav K, Xiao S, Krishna J, Sen S. 2022. Bi-phasic quasistatic brain communication for fully untethered connected brain implants. arXiv:2205.08540 [q-bio.NC]
11. Lee S. 2020. *What is the Internet of Bodies?* Multimed. Video, Rand Corp., Santa Monica, CA. **https://www.rand.org/multimedia/video/2020/10/29/what-is-the-internet-of-bodies.html**
12. Sen S. 2016. Context-aware energy-efficient communication for IoT sensor nodes. In *2016 53nd ACM/EDAC/IEEE Design Automation Conference*, pp. 1–6. New York: ACM
13. Candes EJ, Tao T. 2005. Decoding by linear programming. *IEEE Trans. Inf. Theory* 51(12):4203–15
14. Donoho DL. 2006. Compressed sensing. *IEEE Trans. Inf. Theory* 52(4):1289–306
15. Mosenia A, Jha NK. 2017. A comprehensive study of security of Internet-of-Things. *IEEE Trans. Emerg. Top. Comput.* 5(4):586–602
16. Das D, Ghosh S, Raychowdhury A, Sen S. 2021. EM/power side-channel attack: white-box modeling and signature attenuation countermeasures. *IEEE Des. Test* 38(3):67–75
17. Das D, Maity S, Nasir SB, Ghosh S, Raychowdhury A, Sen S. 2018. ASNI: attenuated signature noise injection for low-overhead power side-channel attack immunity. *IEEE Trans. Circuits Syst. I* 65(10):3300–11
18. Das D, Danial J, Golder A, Modak N, Maity S, et al. 2021. EM and power SCA-resilient AES-256 through >350× current-domain signature attenuation and local lower metal routing. *IEEE J. Solid-State Circuits* 56(1):136–50
19. Das D, Nath M, Chatterjee B, Ghosh S, Sen S. 2019. STELLAR: a generic EM side-channel attack protection through ground-up root-cause analysis. In *2019 IEEE International Symposium on Hardware Oriented Security and Trust*, pp. 11–20. Piscataway, NJ: IEEE
20. Chatterjee B, Das D, Maity S, Sen S. 2019. RF-PUF: enhancing IoT security through authentication of wireless nodes using in-situ machine learning. *IEEE Internet Things J.* 6(1):388–98
21. Bari MF, Chatterjee B, Sivanesan K, Yang LL, Sen S. 2021. High accuracy RF-PUF for EM security through physical feature assistance using public Wi-Fi dataset. In *IEEE MTT-S International Microwave Symposium*, pp. 108–11. Piscataway, NJ: IEEE

22. Moon E, Barrow M, Lim J, Lee J, Nason SR, et al. 2021. Bridging the "last millimeter" gap of brain–machine interfaces via near-infrared wireless power transfer and data communications. *ACS Photon.* 8(5):1430–38
23. Lim J, Lee J, Moon E, Barrow M, Atzeni G, et al. 2021. A light tolerant neural recording IC for near-infrared-powered free floating motes. In *2021 IEEE Symposium on VLSI Circuits*, pp. 1–2. Piscataway, NJ: IEEE
24. Seo D, Carmena JM, Rabaey JM, Maharbiz MM, Alon E. 2015. Model validation of untethered, ultrasonic neural dust motes for cortical recording. *J. Neurosci. Methods* 244:114–22
25. Seo D, Neely RM, Shen K, Singhal U, Alon E, et al. 2016. Wireless recording in the peripheral nervous system with ultrasonic neural dust. *Neuron* 91(3):529–39
26. Ghanbari MM, Piech DK, Shen K, Alamouti SF, Yalcin C, et al. 2019. A 0.8 mm^3 ultrasonic implantable wireless neural recording system with linear AM backscattering. In *2019 IEEE International Solid-State Circuits Conference*, pp. 284–86. Piscataway, NJ: IEEE
27. Ghanbari MM, Piech DK, Shen K, Alamouti SF, Yalcin C, et al. 2019. A sub-mm^3 ultrasonic free-floating implant for multi-mote neural recording. *IEEE J. Solid-State Circuits* 54(11):3017–30
28. Bos T, Dehaene W, Verhelst M. 2019. Ultrasound in-body communication with OFDM through multipath realistic channels. In *2019 IEEE Biomedical Circuits and Systems Conference*, pp. 1–4. Piscataway, NJ: IEEE
29. Bos T, Jiang W, D'hooge J, Verhelst M, Dehaene W. 2019. Enabling ultrasound in-body communication: FIR channel models and QAM experiments. *IEEE Trans. Biomed. Circuits Syst.* 13(1):135–44
30. Ren W, Sun Y, Zhao D, Aili A, Zhang S, et al. 2021. High-performance wearable thermoelectric generator with self-healing, recycling, and Lego-like reconfiguring capabilities. *Sci. Adv.* 7(7):eabe0586
31. Thimot J, Shepard KL. 2017. Bioelectronic devices: wirelessly powered implants. *Nat. Biomed. Eng.* 1:51
32. Lee J, Leung V, Lee AH, Huang J, Asbeck P, et al. 2021. Neural recording and stimulation using wireless networks of microimplants. *Nat. Electron.* 4:604–14
33. Vitale NR, Azin M, Mohseni P. 2018. A Bluetooth low energy (BLE)-enabled wireless link for bidirectional communications with a neural microsystem. In *2018 IEEE Biomedical Circuits and Systems Conference*, pp. 1–4. Piscataway, NJ: IEEE
34. Yu Z, Chen JC, Avants BW, He Y, Singer A, et al. 2020. An 8.2 mm^3 implantable neurostimulator with magnetoelectric power and data transfer. In *2020 IEEE International Solid-State Circuits Conference*, pp. 510–12. Piscataway, NJ: IEEE
35. Alrashdan FT, Chen JC, Singer A, Avants BW, Yang K, Robinson JT. 2021. Wearable wireless power systems for 'ME-BIT' magnetoelectric-powered bio-nodes. *J. Neural Eng.* 18:045011
36. Singer A, Dutta S, Lewis E, Chen Z, Chen JC, et al. 2020. Magnetoelectric materials for miniature, wireless neural stimulation at therapeutic frequencies. *Neuron* 107(4):631–43
37. Marefat F, Erfani R, Kilgore KL, Mohseni P. 2020. A 280 μW 108dB DR readout IC with wireless capacitive powering using a dual-output regulating rectifier for implantable PPG recording. In *2020 IEEE International Solid-State Circuits Conference*, pp. 412–14. Piscataway, NJ: IEEE
38. Erfani R, Marefat F, Nag S, Mohseni P. 2019. A 1–10-MHz frequency-aware CMOS active rectifier with dual-loop adaptive delay compensation and >230-mW output power for capacitively powered biomedical implants. *IEEE J. Solid-State Circuits* 55(3):756–66
39. Koruprolu A, Nag S, Erfani R, Mohseni P. 2018. Capacitive wireless power and data transfer for implantable medical devices. In *2018 IEEE Biomedical Circuits and Systems Conference*, pp. 1–4. Piscataway, NJ: IEEE
40. Li J, Dong Y, Park JH, Lin L, Tang T, et al. 2020. Human-body-coupled power-delivery and ambient-energy-harvesting ICs for a full-body-area power sustainability. In *2020 IEEE International Solid-State Circuits Conference*, pp. 514–16. Piscataway, NJ: IEEE
41. Li J, Dong Y, Park JH, Yoo J. 2021. Body-coupled power transmission and energy harvesting. *Nat. Electron.* 5:530–38
42. Modak N, Das D, Nath M, Chatterjee B, Gaurav K, et al. 2021. A 65 nm resonant electro-quasistatic 5–240 μW human whole-body powering and 2.19 μW communication SoC with automatic maximum resonant power tracking. In *2021 IEEE Custom Integrated Circuits Conference*, pp. 1–2. Piscataway, NJ: IEEE

43. Modak N, Das D, Nath M, Chatterjee B, Gaurav K, et al. 2022. EQS Res-HBC: a 65-nm electro-quasistatic resonant 5–240 μW human whole-body powering and 2.19 μW communication SoC with automatic maximum resonant power tracking. *IEEE J. Solid-State Circuits* 57(3):831–44
44. Cho H, Suh J-H, Kim C, Ha S, Je M. 2022. An intra-body power transfer system with >1-mW power delivered to the load and 3.3-V dc output at 160 cm of on-body distance. *IEEE Trans. Biomed. Circuits Syst.* 16(5):852–66
45. Makowski NS, Campean A, Lambrecht JM, Buckett JR, Coburn JD, et al. 2021. Design and testing of stimulation and myoelectric recording modules in an implanted distributed neuroprosthetic system. *IEEE Trans. Biomed. Circuits Syst.* 15(2):281–93
46. CMS (US Cent. Medicare Medicaid Serv.). 2019. *National health expenditure data*. Data Sets, CMS, Washington, DC. **https://www.cms.gov/Research-Statistics-Data-and-Systems/Statistics-Trends-and-Reports/NationalHealthExpendData/NationalHealthAccountsHistorical**
47. Zhang M, Chan C, Zhu Y, Martins RP. 2019. A 0.6-V 13-bit 20-MS/s two-step TDC-assisted SAR ADC with PVT tracking and speed-enhanced techniques. *IEEE J. Solid-State Circuits* 54(12):3396–409
48. Chatterjee B, Srivastava A, Seo DH, Yang D, Sen S. 2020. A context-aware reconfigurable transmitter with 2.24 pJ/bit, 802.15.6 NB-HBC and 4.93 pJ/bit, 400.9 MHz MedRadio modes with 33.6% transmit efficiency. In *2020 IEEE Radio Frequency Integrated Circuits Symposium*, pp. 75–78. Piscataway, NJ: IEEE
49. Singer A, Robinson JT. 2021. Wireless power delivery techniques for miniature implantable bioelectronics. *Adv. Healthc. Mater.* 10(17):2100664
50. Yazicioglu RF, Merken P, Puers R, Van Hoof C. 2007. A 60 μW 60 nV/$\sqrt{\text{Hz}}$ readout front-end for portable biopotential acquisition systems. *IEEE J. Solid-State Circuits* 42(5):1100–10
51. Enz CC, Temes GC. 1996. Circuit techniques for reducing the effects of op-amp imperfections: autozeroing, correlated double sampling, and chopper stabilization. *Proc. IEEE* 84(11):1584–14
52. Denison T, Consoer K, Santa W, Avestruz AT, Cooley J, Kelly A. 2007. A 2 μW 100 nV/$\sqrt{\text{Hz}}$ chopper-stabilized instrumentation amplifier for chronic measurement of neural field potentials. *IEEE J. Solid-State Circuits* 42(12):2934–45
53. Chandrakumar H, Marković D. 2017. A high-dynamic-range neural recording chopper amplifier for simultaneous neural recording and stimulation. *IEEE J. Solid-State Circuits* 52(3):645–56
54. Mehrotra P, Chatterjee B, Sen S. 2019. EM-wave biosensors: a review of RF, microwave, mm-wave and optical sensing. *Sensors* 19(5):1013
55. Murmann B. 2022. *ADC performance survey 1997–2022*. Data Set, GitHub. **https://github.com/bmurmann/ADC-survey**
56. Chatterjee B, Mousoulis C, Maity S, Kumar A, Scott S, et al. 2019. A wearable real-time CMOS dosimeter with integrated zero-bias floating gate sensor and an 861-nW 18-bit energy-resolution scalable time-based radiation to digital converter. In *2019 IEEE Custom Integrated Circuits Conference*, pp. 1–4. Piscataway, NJ: IEEE
57. Chatterjee B, Mousoulis C, Seo DH, Kumar A, Maity S, et al. 2020. A wearable real-time CMOS dosimeter with integrated zero-bias floating gate sensor and an 861-nW 18-bit energy-resolution scalable time-based radiation to digital converter. *IEEE J. Solid-State Circuits* 55(3):650–65
58. Lustig M, Donoho D, Pauly JM. 2007. Sparse MRI: the application of compressed sensing for rapid MR imaging. *Magn. Reson. Med.* 58(6):1182–95
59. Anvesha A, Xu S, Romberg J, Raychowdhury A. 2017. A 130 nm 165 nJ/frame compressed-domain smashed-filter based mixed-signal classifier for "in-sensor" analytics in smart cameras. *Trans. Circuits Syst. II* 65(3):296–300
60. Zhang J, Wang Z, Verma N. 2015. A matrix-multiplying ADC implementing a machine-learning classifier directly with data conversion. In *2015 IEEE International Solid-State Circuits Conference*, pp. 1–3. Piscataway, NJ: IEEE
61. Anvesha A, Xu S, Romberg J, Raychowdhury A. 2017. A 65 nm compressive-sensing time-based ADC with embedded classification and INL-aware training for arrhythmia detection. In *2017 IEEE Biomedical Circuits and Systems Conference*, pp. 1–4. Piscataway, NJ: IEEE
62. Gaurav K, Chatterjee B, Sen S. 2021. A 16 pJ/bit 0.1–15 Mbps compressive sensing IC with on-chip DWT sparsifier for audio signals. In *2021 IEEE Custom Integrated Circuits Conference*, pp. 1–2. Piscataway, NJ: IEEE

63. Gaurav K, Chatterjee B, Sen S. 2021. CS-audio: a 16 pJ/b 0.1–15 Mbps compressive sensing IC with DWT sparsifier for audio-AR. *IEEE J. Solid-State Circuits* 57(7):2220–35
64. Qaisar S, Bilal RM, Iqbal W, Naureen M, Lee S. 2013. Compressive sensing: from theory to applications. A survey. *J. Commun. Netw.* 15(5):443–56
65. Hamza D, Abbes A, Faycal B. 2018. Compressive sensing–based IoT applications: a review. *J. Sens. Actuator Netw.* 7(4):45
66. Roose JD, Xin H, Andraud M, Harpe PJA, Verhelst M. 2018. Flexible and self-adaptive sense-and-compress for sub-microwatt always-on sensory recording. In *2018 IEEE 44th European Solid State Circuits Conference*, pp. 282–85. Piscataway, NJ: IEEE
67. Trakimas M, Sonkusale SR. 2011. An adaptive resolution asynchronous ADC architecture for data compression in energy constrained sensing applications. *IEEE Trans. Circuits Syst. I* 58(5):921–34
68. Ieong C, Li M, Law M, Mak P, Vai MI, Martins RP. 2017. A 0.45 V 147–375 nW ECG compression processor with wavelet shrinkage and adaptive temporal decimation architectures. *IEEE Trans. VLSI Syst.* 25(4):1307–19
69. Naderiparizi S, Hessar M, Talla V, Gollakota S, Smith JR. 2018. Towards battery-free HD video streaming. In *2018 15th USENIX Symposium on Networked Systems Design and Implementation*, pp. 233–47. Piscataway, NJ: IEEE
70. Chatterjee B, Gaurav K, Xiao S, Barik G, Krishna J, Sen S. 2022. A 1.8 μW 5.5 mm^3 ADC-less neural implant SoC utilizing 13.2 pJ/sample time-domain bi-phasic quasi-static brain communication with direct analog to time conversion. In *2022 European Conference on Solid-State Circuits*, pp. 209–12. Piscataway, NJ: IEEE
71. Li W, Bao J, Shen W. 2011. Collaborative wireless sensor networks: a survey. In *2011 IEEE International Conference on Systems, Man, and Cybernetics*, pp. 2614–19. Piscataway, NJ: IEEE
72. Buehrer RM, Wymeersch H, Vaghefi RM. 2018. Collaborative sensor network localization: algorithms and practical issues. *Proc. IEEE* 106(6):1089–114
73. Chang G, Maity S, Chatterjee B, Sen S. 2018. A MedRadio receiver front-end with wide energy-quality scalability through circuit and architecture-level reconfigurations. *IEEE J. Emerg. Sel. Top. Circuits Syst.* 8(3):369–78
74. Cao N, Chatterjee B, Liu, Cheng B, Gong M, et al. 2022. A 65 nm wireless image SoC supporting on-chip DNN optimization and real-time computation-communication trade-off via actor-critical neuro-controller. *IEEE J. Solid-State Circuits* 57(8):2545–59
75. Maity S, Chatterjee B, Chang G, Sen S. 2019. BodyWire: a 6.3-pJ/b 30-Mb/s 30-dB SIR-tolerant broadband interference-robust human body communication transceiver using time domain interference rejection. *IEEE J. Solid-State Circuits* 54(10):2892–906
76. Mondal S, Hall DA. 2020. A 67-μW ultra-low power PVT-robust MedRadio transmitter. In *2020 IEEE Radio Frequency Integrated Circuits Symposium*, pp. 327–30. Piscataway, NJ: IEEE
77. Lucev Ž, Krois I, Cifrek M. 2012. A capacitive intrabody communication channel from 100 kHz to 100 MHz. *IEEE Trans. Instrum. Meas.* 61(12):3280–89
78. Bae J, Cho H, Song K, Lee H, Yoo HJ. 2012. The signal transmission mechanism on the surface of human body for body channel communication. *IEEE Trans. Microw. Theory Tech.* 60(3):582–93
79. Park J, Garudadri H, Mercier PP. 2017. Channel modeling of miniaturized battery-powered capacitive human body communication systems. *IEEE Trans. Biomed. Eng.* 64(2):452–62
80. Maity S, He M, Nath M, Das D, Chatterjee B, Sen S. 2019. Bio-physical modeling, characterization, and optimization of electro-quasistatic human body communication. *IEEE Trans. Biomed. Eng.* 66(6):1791–802
81. Nath M, Maity S, Sen S. 2020. Toward understanding the return path capacitance in capacitive human body communication. *IEEE Trans. Circuits Syst. II* 67(10):1879–83
82. Maity S, Das D, Chatterjee B, Sen S. 2018. Characterization and classification of human body channel as a function of excitation and termination modalities. In *2018 Annual International Conference of the IEEE Engineering in Medicine and Biology Society*, pp. 3754–57. Piscataway, NJ: IEEE
83. Chatterjee B, Datta A, Nath M, Gaurav K, Modak N, Sen S. 2022. A 65 nm 63.3 μW 15 Mbps transceiver with switched-capacitor adiabatic signaling and combinatorial-pulse-position modulation for

body-worn video-sensing AR nodes. In *2022 IEEE International Solid-State Circuits Conference*, pp. 276–78. Piscataway, NJ: IEEE
84. Modak N, Nath M, Chatterjee B, Maity S, Sen S. 2022. Bio-physical modeling of galvanic human body communication in electro-quasistatic regime. *IEEE Trans. Biomed. Eng.* 69(12):3717–27
85. Park J, Mercier PP. 2015. Magnetic human body communication. In *2015 Annual International Conference of the IEEE Engineering in Medicine and Biology Society*, pp. 1841–44. Piscataway, NJ: IEEE
86. Park J, Mercier PP. 2019. A sub-40 μW 5 Mb/s magnetic human body communication transceiver demonstrating trans-body delivery of high-fidelity audio to a wearable in-ear headphone. In *2019 IEEE International Solid-State Circuits Conference*, pp. 1841–44. Piscataway, NJ: IEEE
87. Nath M, Ulvog AK, Weigand S, Sen S. 2021. Understanding the role of magnetic and magneto-quasistatic fields in human body communication. arXiv:2011.00125 [eess.SP]
88. Tochou G, Benarrouch R, Gaidioz D, Cathelin A, Frappé A, et al. 2022. A sub-100-μW 0.1-to-27-Mb/s pulse-based digital transmitter for the human intranet in 28-nm FD-SOI CMOS. *IEEE J. Solid-State Circuits* 57(5):1409–20
89. Lee M-C, Karimi-Bidhendi A, Malekzadeh-Arasteh O, Wang PT, Do AH, et al. 2019. A CMOS MedRadio transceiver with supply-modulated power saving technique for an implantable brain–machine interface system. *IEEE J. Solid-State Circuits* 54(6):1541–52
90. Jaussi JE, Balamurugan G, Hyvonen S, Hsueh TC, Musah T, et al. 2014. A 205 mW 32 Gb/s 3-tap FFE/6-tap DFE bidirectional serial link in 22 nm CMOS. In *2014 IEEE International Solid-State Circuits Conference*, pp. 440–41. Piscataway, NJ: IEEE
91. Hsueh TC, Balamurugan G, Jaussi JE, Hyvonen S, Kennedy J, et al. 2014. A 25.6 Gb/s differential and DDR4/GDDR5 dual-mode transmitter with digital clock calibration in 22 nm CMOS. In *2014 IEEE International Solid-State Circuits Conference*, pp. 444–45. Piscataway, NJ: IEEE
92. Cao N, Nasir SB, Sen S, Raychowdhury A. 2017. In-sensor analytics and energy-aware self-optimization in a wireless sensor node. In *IEEE MTT-S International Microwave Symposium*, pp. 200–3. Piscataway, NJ: IEEE
93. Chatterjee B, Panda P, Maity S, Biswas A, Roy K, Sen S. 2019. Exploiting inherent error resiliency of deep neural networks to achieve extreme energy efficiency through mixed-signal neurons. *IEEE Trans. VLSI Syst.* 27(6):1365–77
94. Chatterjee B, Sen S. 2021. Energy-efficient deep neural networks with mixed-signal neurons and dense-local and sparse-global connectivity. In *2021 26th Asia and South Pacific Design Automation Conference*, pp. 297–304. Piscataway, NJ: IEEE
95. Ebrazeh A, Mohseni P. 2015. 30 pJ/b, 67 Mbps, centimeter-to-meter range data telemetry with an IR-UWB wireless link. *IEEE Trans. Biomed. Circuits Syst.* 9(3):362–69
96. Sarpeshkar R. 1998. Analog versus digital: extrapolating from electronics to neurobiology. *Neural Comput.* 10(7):1601–38
97. Sodagar AM, Perlin GE, Yao Y, Najafi K, Wise KD. 2009. An implantable 64-channel wireless microsystem for single-unit neural recording. *IEEE J. Solid-State Circuits* 44(9):2591–604
98. Hosseini-Nejad H, Jannesari A, Sodagar AM. 2014. Data compression in brain–machine/computer interfaces based on the Walsh–Hadamard transform. *IEEE Trans. Biomed. Circuits Syst.* 8(1):129–37
99. Lim J, Moon E, Barrow M, Nason SR, Patel PR, et al. 2020. A 0.19×0.17 mm^2 wireless neural recording IC for motor prediction with near-infrared-based power and data telemetry. In *2020 IEEE International Solid-State Circuits Conference*, pp. 416–18. Piscataway, NJ: IEEE
100. Schwartz AB. 2004. Cortical neural prostheses. *Annu. Rev. Neurosci.* 27:487–507
101. Taylor DM, Tillery IH, Schwartz AB. 2003. Information conveyed through brain control: cursor versus robot. *IEEE Trans. Neural Syst. Rehabil. Eng.* 11:195–99
102. Olsson RH, Wise KD. 2005. A three-dimensional neural recording microsystem with implantable data compression circuitry. *IEEE J. Solid-State Circuits* 40(12):2796–804
103. Harrison R, Watkins PT, Kier RJ, Lovejoy RO, Black DJ, et al. 2007. A low-power integrated circuit for a wireless 100-electrode neural recording system. *IEEE J. Solid-State Circuits* 42(1):123–33
104. Craciun S, Cheney D, Gugel K, Sanchez JC, Principe JC. 2011. Wireless transmission of neural signals using entropy and mutual information compression. *IEEE Trans. Neural Syst. Rehabil. Eng.* 19(1):35–44

105. Shoaib M, Jha NK, Verma N. 2012. Enabling advanced inference on sensor nodes through the direct use of compressively-sensed signals. In *2012 IEEE Design, Automation & TEST in Europe Conference*, pp. 437–43. Piscataway, NJ: IEEE
106. Dixon AMR, Allstot EG, Gangopadhyay D, Allstot DJ. 2012. Compressed sensing system considerations for ECG and EMG wireless biosensors. *IEEE Trans. Biomed. Circuits Syst.* 6(2):156–66
107. Zamani H, Bahrami HR, Chalwadi P, Garris PA, Mohseni P. 2018. C-FSCV: compressive fast-scan cyclic voltammetry for brain dopamine recording. *IEEE Trans. Neural Syst. Rehabil. Eng.* 26(1):51–59
108. Kamboh AM, Raetz M, Oweiss KG, Mason A. 2007. Area-power efficient VLSI implementation of multichannel DWT for data compression in implantable neuroprosthetics. *IEEE Trans. Biomed. Circuits Syst.* 1(2):128–35
109. Yang Y, Kamboh AM, Mason AJ. 2010. Adaptive threshold spike detection using stationary wavelet transform for neural recording implants. In *2010 IEEE Biomedical Circuits and Systems Conference*, pp. 9–12. Piscataway, NJ: IEEE
110. Irwin ZT, Thompson DE, Schroeder KE, Tat DM, Hassani A, et al. 2016. Enabling low-power, multimodal neural interfaces through a common, low-bandwidth feature space. *IEEE Trans. Neural Syst. Rehabil. Eng.* 24(5):521–31
111. Wang W, Zhu L, Marefat F, Mohseni P, Kilgore K, Najafizadeh L. 2020. Photoplethysmography-based blood pressure estimation using deep learning. In *2020 Asilomar Conference on Signals, Systems, and Computers*, pp. 945–49. Piscataway, NJ: IEEE
112. Wang W, Mohseni P, Kilgore K, Najafizadeh L. 2021. Cuff-less blood pressure estimation via small convolutional neural networks. In *2021 43rd Annual International Conference of the IEEE Engineering in Medicine and Biology Society*, pp. 1031–34. Piscataway, NJ: IEEE
113. Thomson I. 2017. AES-256 keys sniffed in seconds using $200 kit a few inches away. *The Register*, June 23. **https://www.theregister.co.uk/2017/06/23/aes_256_cracked_50_seconds_200_kit**
114. Das D, Danial J, Golder A, Modak N, Maity S, et al. 2020. 27.3 EM and power SCA-resilient AES-256 in 65 nm CMOS through >350× current-domain signature attenuation. In *2020 IEEE International Solid-State Circuits Conference*, pp. 424–26. Piscataway, NJ: IEEE
115. Ghosh A, Das D, Danial J, De V, Ghosh S, Sen S. 2021. An EM/power SCA-resilient AES-256 with synthesizable signature attenuation using digital-friendly current source and RO-bleed-based integrated local feedback and global switched-mode control. In *2021 IEEE International Solid-State Circuits Conference*, pp. 499–501. Piscataway, NJ: IEEE

Annual Review of Biomedical Engineering

Volume 25, 2023

Contents

Errata

An online log of corrections to *Annual Review of Biomedical Engineering* articles may be found at http://www.annualreviews.org/errata/bioeng